Published in *Stochastic Processes in Physics, Chemistry and Biology*, eds. J. A. Freund and T. Poeschel, Springer, Berlin, 2000, pp 378-389.

Fluctuational escape from a chaotic attractor

Igor A. Khovanov[1], Dmitri G. Luchinsky[2], Riccardo Mannella[3], and Peter V.E. McClintock[2]

[1] Department of Physics, Saratov State University, Astrahanskaya 83, 410026, Saratov, Russia
[2] Department of Physics, Lancaster University, Lancaster, LA1 4 YB, UK
[3] Dipartimento di Fisica, Università di Pisa and INFM UdR Pisa, Piazza Torricelli 2, 56100 Pisa, Italy

Abstract. Noise-induced escape from a non-hyperbolic attractor, and from a quasi-hyperbolic attractor with nonfractal boundaries, is investigated by means of analogue experiments and numerical simulations. It is found that there exists a most probable (optimal) escape trajectory, the prehistory of the escape being defined by the structure of the chaotic attractor. The corresponding optimal fluctuational force is found. The possibility of achieving analytic estimates of the escape probability within the framework of Hamiltonian formalism is discussed.

1 The escape problem for chaotic systems

There have been recently a number of interesting studies of the interplay of noise with chaotic behaviour [1, 2] including e.g. a demonstration of chaotic features in a purely stochastic Kramers oscillator [3], the phenomena of both noise-induced instability [4] and noise-induced order [5], noise-induced chaos [6] and quantum noise-induced chaotic oscillations [7]. However, the analytic estimation of the probability of noise-induced escape from the basin of attraction of a chaotic attractor remains an unsolved fundamental problem in the theory of fluctuations [8, 9]. It is of broad interdisciplinary interest in view of a host of important applications including e.g. stabilisation of the voltage standard [10], neuron dynamics [11], and laser systems [12].

It has now been established, however, that the fluctuational dynamics of escape can be investigated directly through measurements of the *prehistory probability distribution* [13–16]. The underlying idea is based on the concept of large fluctuations [17], in which the system fluctuates to the remote state along an *optimal path*. Mathematical equivalents of this physical concept are asymptotic equations for the solution of the Fokker-Plank equation written in the form of rays (Hamilton equations), or wavefronts (Hamilton-Jacobi equation) [18]. In this method the dynamical variables of the system, and sometimes also the external force, are recorded simultaneously, and the statistics of all actual trajectories along which system evolves to a given state are then analyzed [13]. The advantages of this technique were demonstrated

earlier [15, 16, 21] by investigation of some fundamental symmetry properties of optimal trajectories and the singularities in their distribution.

In the present paper we use measurements of the prehistory probability distribution for the direct experimental investigation of fluctuational escape from a chaotic attractor and discuss the possibility of achieving analytic estimates of the escape probability within the framework of Hamiltonian formalism in the context of our results. We study two systems with different attractors: a non-hyperbolic attractor in a nonautonomous nonlinear oscillator; and a quasi-hyperbolic attractor in the Lorenz system.

2 Escape from a non-hyperbolic attractor

2.1 The model

We first investigated the stochastic dynamics of a periodically driven nonlinear oscillator with equation of motion

$$\begin{aligned} \dot{\mathbf{q}} &= \mathbf{K}(\mathbf{q},t) + \mathbf{f}(t), \\ \mathbf{K} &= \{K_1, K_2\} = \{q_2, -2\Gamma q_2 - \omega_0^2 q_1 - \beta q_1^2 - \gamma q_1^3 + h\sin(\omega_f t)\}, \\ \mathbf{f}(t) &= \{0, \xi(t)\}, \quad \langle \xi(t)\rangle = 0, \quad \langle \xi(t)\xi(0)\rangle = D\delta(t) = 4\Gamma kT\delta(t), \\ \Gamma &\ll \omega_f, \quad \frac{9}{10} < \frac{\beta^2}{\gamma\omega^2} < 4. \end{aligned} \tag{1}$$

Parameters were chosen so that the potential is monostable ($\beta^2 < 4\gamma\omega_0^2$) and the dependence of the energy of oscillations on the frequency is non-monotonic ($\frac{\beta^2}{\gamma\omega_0^2} > \frac{9}{10}$). This model is encountered in many applications and allows a theoretical analysis to be carried out over a wide range of parameter values (see e.g. [22–24]). It was shown earlier [23] that chaos in (1) arises for relatively small driving force amplitudes $h \approx 0.1$.

A simplified bifurcation diagram obtained by numerical simulation is shown in Fig. 1a. Boundaries of the hysteresis of the period 1 resonance are shown by full lines, and those of the period 2 resonance by dotted lines. Chaotic states are indicated by small pluses. The region of coexistence of the two period-2 resonances is bounded by the dash-dotted line.

The bifurcation diagram shown in Fig. 1b for one set of parameters explains some of the notation used in Fig. 1a. Thus arrows 3 and 9 indicate the boundaries of stability of the large stable limit cycle of period 1 and correspond to the filled circles in the Fig. 1a. In particular it can be seen: that there are two coexisting limit cycles of period 2; and that the chaotic state appears via a sequence of period-doubling bifurcations and thus corresponds to a non-hyperbolic attractor [25], i.e. to a chaotic attractor (CA) consisting of both stable and unstable sets.

We note that the bifurcation diagram shown in Fig. 1a is in qualitative agreement with earlier theoretical predictions [23]. The working point P was

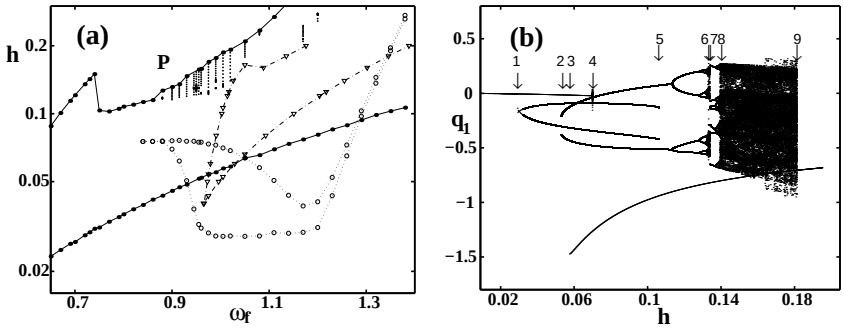

Fig. 1. (**a**) A two-dimensional bifurcation diagram of the system (1) on the (ω_f, h) plane obtained from numerical simulations with $\Gamma = 0.025, \omega_0 = 0.597, \beta = 1, \gamma = 1$. Regions of chaos are shown by crosses. Regions where two attractors corresponding to the resonances of period 1 coexist are shown by dots. Circles indicate the boundaries of the hysteresis corresponding to the period 2 resonance. The region where two period 2 attractors coexist is shown by triangles (the full, dashed-dotted and dashed lines are guides to the eye). The working point P with $\omega_f = 0.95, h = 0.13$ shown by bold plus was placed in the region of coexistence of the period 1 stable limit cycle and of the chaotic attractor. (**b**) A bifurcation diagram obtained in Poincaré cross-section for $t = n\omega_f/2\pi, n = 0, 1..., \omega_f = 1.005$ shows values of q_1 as a function of amplitude h. Arrows 1 and 4 indicate the region of hysteresis for the period 2 resonance corresponding to the circles in Fig. 1a. The region of coexistence of the two resonances of period 2 is shown by arrows 2 and 5 corresponding to the triangle in Fig. 1a. The hysteresis for the large stable limit cycle of period 1 is indicated by arrows 3 and 9 corresponding to the filled dots in Fig. 1a. Arrows 6-9 show the boundaries of the chaotic states

chosen to lie in the region where the chaotic attractor coexists with the stable limit cycle. This regime is often of interest from the point of view of applications (see e.g. [11, 26–28]).

The escape process has been studied through both analogue electronic [29] and digital simulations. The latter employed the prescriptions of [30], given that simulation times necessarily grow exponentially as $T \to 0$. Both techniques yielded qualitatively similar results, but the data shown here are digital, because precision is of particular importance. The basins of attraction of the coexisting chaotic attractor CA and large stable limit cycle SC1 are shown in Fig. 2 for the Poincaré cross-section $\omega_f t = 0.6\pi (\mathrm{mod}\, 2\pi)$ in the absence of noise. The value of the maximal Lyapunov exponent for the CA is 0.0449. The symbols UC1 in the figure denote saddle cycle of period 1 which lies on the boundary between the basins of attraction of CA. The stable manifolds of cycle UC1 define the boundary of basins.

In the presence of noise there is a finite probability of noise-induced transitions between CA and SC1. The intersections of one of the actual escape trajectories are shown in Poincaré cross-section by the filled circles. The sad-

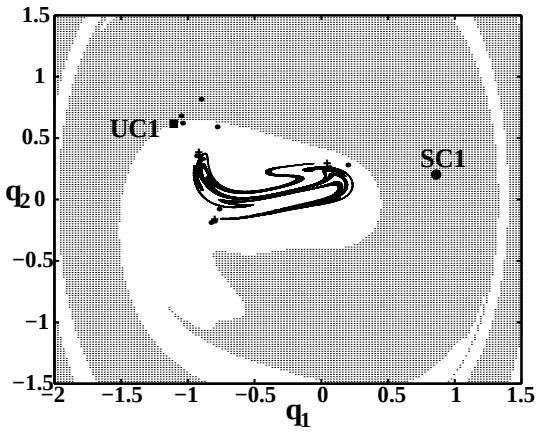

Fig. 2. The basins of attraction of the stable limit cycle SC1 (shaded) and CA (white) for a Poincaré cross-section with $\omega_f t = 0.6\pi(mod 2\pi)$, $\omega_f = 0.95$. The saddle cycle of period 1 UC1 is shown by the filled square, and that of period 3 UC3 by the pluses. Intersections of the actual escape trajectory with the Poincaré cross-section are indicated by the filled circles.

dle cycle of period 3 UC3 is shown in the figure by pluses. Multipliers for UC3 are $\mu_1 = 0.04873 < 1$ and $\mu_2 = 7.608312 > 1$. It is evident that the actual escape trajectory passes very close to UC3 (see also below).

2.2 Theoretical approach

In the limit of small noise intensity, deep insight into the fluctuational dynamics of escape can be gained within the framework of Hamiltonian formalism. To appreciate what physical picture of escape from CA might be expected, we first consider the simpler process of escape from a stable limit cycle SC bounded by an unstable cycle UC. The system will spend most of its time fluctuating in the close vicinity of the limit cycle, only occasionally fluctuating far away towards the boundary of its basin of attraction. But when these large rare fluctuations do arise, they occur in almost deterministic way: escape from a domain of attraction typically occurs along a *unique trajectory* (see e.g. [31–34]). For the stable limit cycle this physical picture was confirmed in numerical simulations [10, 26]. In general the escape will take place along the unique most probable escape path (MPEP). The probability of escape along the MPEP $\rho(\mathbf{q})$ in the limit of small noise intensity can be written in the form [18] (see also [13, 15–21])

$$\rho(\mathbf{q}) \approx constant \times \exp(-S(\mathbf{q})/kT), \quad T \to 0. \tag{2}$$

$S(\mathbf{q})$ is an "activation energy" of fluctuations to the vicinity of the point $\mathbf{q}$ in the system state space. Expression (2) is an analogue of the WKB

approximation for the corresponding to (1) Fokker-Plank equation.

$$\dot{\rho} = 2\Gamma\nabla^2\rho - \nabla\cdot(\rho\mathbf{K}). \tag{3}$$

$S(\mathbf{q})$ may be viewed as a *classical action*, because to leading order it satisfies an eikonal (Hamilton–Jacobi) equation of the form

$$\dot{S} + H\left(\mathbf{q}, \frac{\partial S}{\partial q}\right) = 0, \qquad H = 2\Gamma p_2^2 + p_1 K_1 + p_2 K_2, \tag{4}$$
$$\dot{\mathbf{q}} = \frac{\partial H}{\partial \mathbf{p}}, \qquad \dot{\mathbf{p}} = -\frac{\partial H}{\partial \mathbf{q}}, \qquad \dot{S} = \frac{1}{2}\mathbf{p}^2, \qquad \mathbf{p} = \{p_1, p_2\} = \frac{\partial S}{\partial \mathbf{q}},$$

where H is a so-called Wentzel–Freidlin Hamiltonian [18]. The optimal fluctuational trajectories are projections onto the coordinate space of the classical trajectories determined by this Hamiltonian. They correspond to extreme values of the action functional in the form [35]

$$S[\mathbf{q}(t)] = \int_{t_f}^{t_f} \frac{1}{2}[\dot{\mathbf{q}}(t) - \mathbf{K}(\mathbf{q}(t))]^2 dt. \tag{5}$$

In general, the computation of the most probable escape path $\mathbf{q}_{opt}(t)$ requires a minimization over the set of the extreme trajectories which spiral from the stable limit cycle SC $\mathbf{q}_{SC}$ (at $t_i \to -\infty$) to the unstable cycle UC $\mathbf{q}_{UC}$ (at $t_f \to \infty$). This trajectory may be found as the solution of a boundary problem for the system (4) with the corresponding boundary conditions in the form

$$\frac{\delta S[\mathbf{q}]}{\delta \mathbf{q}(t)} = 0, \qquad \begin{cases} \mathbf{q}(t_i) \to \mathbf{q}_{SC}, \ \mathbf{p}(t_i) \to 0 & \text{for } t_i \to -\infty \\ \mathbf{q}(t_f) \to \mathbf{q}_{UC}, \ \mathbf{p}(t_f) \to 0 & \text{for } t_f \to \infty \end{cases} \tag{6}$$

Thus the MPEP is a heteroclinic trajectory of *least* action of the Hamiltonian dynamical system associated with (1).

In fact, equations (4) describe *extreme* fluctuational paths. *Optimal* paths provide the *global* minimum to the action $S[\mathbf{q}]$. It is clear from (2) that, for small T, it is these optimal paths that possess physical significance; extreme paths are not necessarily physically significant. For small noise intensity, the probability of escape along the MPEP is exponentially small; but it is exponentially more probable then the probability of escape along any other trajectory, including the other heteroclinic trajectories of (4). This is the optimal path observed in a physical experiment.

2.3 Experimental approach

To investigate the dynamics of large fluctuations one may use an experimental approach in which one accumulates information about all arrivals of the system in the close vicinity of a chosen state $\mathbf{q}_f$. In our experimental technique [13] we monitor continuously the dynamical variables (q_1,q_2), and the

random force ξ, until noise-induced escape takes place. We store the relevant part of the escape trajectory and noise realization ($q_1^{es}(t)$,$q_2^{es}(t)$, $\xi^{es}(t)$), and then reset the system once more to the chaotic attractor. An ensemble-average of such trajectories built up over a period of continuous monitoring creates the *prehistory probability distribution* [13] $p_h(\mathbf{q}, t; \mathbf{q}_f, t_f)$. Note that it differs from the ordinary conditional probability distribution and that it sets optimal paths into a physical context: their physical significance follows from the fact that $p_h(\mathbf{q}, t; \mathbf{q}_f, t_f)$ at any given moment of time t should have a sharp maximum in $\mathbf{q}$ lying on the optimal path, $\mathbf{q} = \mathbf{q}_{opt}(t|t_f, \mathbf{q}_f)$; and the optimal path is in fact just the $D \to 0$ limit of the ridges of the prehistory distribution. By investigating the prehistory probability distribution experimentally, one can establish the area of phase space within which optimal paths are well defined, i.e. where the tube of fluctuational paths around an optimal path is narrow. The prehistory distribution thus provides information about both the optimal path and the probability that it will be followed.

We note that the existence of most probable escape trajectories, as well as the validity of the eqs. (2,4) was confirmed earlier in analogue experiments for a number of non-chaotic systems(see e.g. [15, 16, 21] and references therein).

2.4 Results of the experimental approach

We now return to consideration of escape from a basin of attraction of CA. Since the the basin of attraction is bounded by the same saddle cycle UC1 one may expect that near the UC1 the situation will be qualitatively the same and that there exists a unique MPEP near UC1. The situation is qualitatively different near a chaotic attractor. Analysis of the Hamiltonian flow in this region is practically impossible and there are no predictions about the character of the distribution of the optimal trajectories near a non-hyperbolic attractor. According to the simplest scenario the MPEP smears out near CA and no unique escape path exists in this region. However, a statistical analysis of actual fluctuational trajectories reveals a different and much more detailed physical picture of the noise-induced escape from a CA.

We have investigated some thousands of actual escape trajectories for the system (1), for different sets of parameters. Fig. 3a presents typical results for the parameter values corresponding to the operating point P shown in the Fig. 1a and a noise intensity $T \approx 0.001$. The most probable escape paths found in the experiment are shown in Fig. 3a by the dotted, dashed and full lines. The probability of escape along first path (dotted) is in 9.5 and 2.375 times larger then escape along the second (dashed) or third (full) paths respectively. All the escape paths merge at the saddle cycle of period 3 UC3. If the noise intensity is reduced further one of the escape paths becomes exponentially more probable then the others. In what follows we concentrate on the properties of this most probable first escape path.

Fig. 3a also shows (thin full lines) 15 measured fluctuational escape trajectories corresponding to an optimal path. All the actual trajectories were

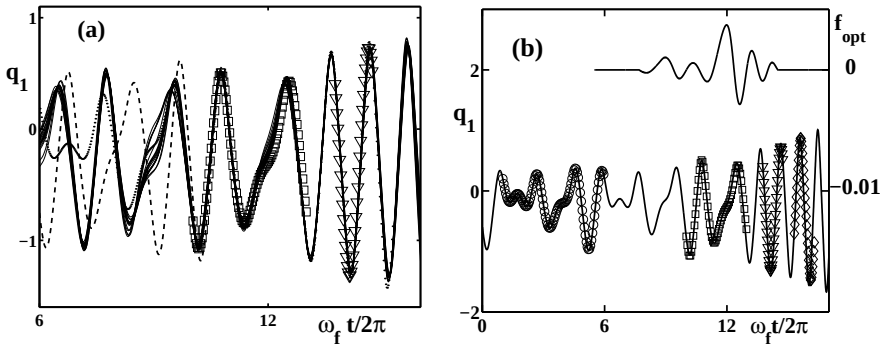

Fig. 3. (**a**) Three optimal escape trajectories from the non-hyperbolic attractor to the stable limit cycle, found in numerical simulations with $T \approx 0.001$, are shown by the full, dashed, and dotted lines respectively. The triangles and filled circles show one period each of the unstable saddle cycles of period 3 (UC3) and 1 (UC1), respectively. The thin full lines show 15 real escape trajectories corresponding to the same optimal trajectory. (**b**) The most probable escape path from the non-hyperbolic attractor to the stable limit cycle, found by use of the prehistory probability distribution for $T \approx 0.0005$, is shown by the full line. Single periods of the unstable saddle cycles of period 5, 3 and 1 are shown by open circles, squares and triangles respectively; the stable limit cycle is shown by rhombs. Parameters used for the simulations in both (**a**) and (**b**) were $h = 0.13$, $\omega_f \approx 0.95$, $\omega_0 \approx 0.597$.

shifted in time so that the characteristic regions of the trajectories corresponding to the transition from chaotic to regular motion coincide with each other. It can be seen from the figure that these trajectories follow closely one and the same optimal escape path. Because of this fact it is possible to determine the optimal escape path by simple averaging.

A statistical analysis of the data – the actual fluctuational trajectories [29] and corresponding noise realizations – reveals the following scenario of escape from the basin of attraction of the non-hyperbolic attractor (see Fig. 3b). The system comes first to UC5, the saddle cycle of period 5 embedded in CA, and then slides down the unstable manifold of this cycle. At this moment the system is driven by noise to the period 3 saddle cycle UC3, which is not part of the non-hyperbolic attractor and can be considered as its boundary. Next, the fluctuations drive the system from the period 3 saddle cycle to the boundary of the basin of attraction of CA. Thus the problem of escape from a non-hyperbolic attractor can be considered in terms of fluctuational transitions between a few saddle cycles of low period, UC5 $\rightarrow$ UC3 $\rightarrow$ UC1. The results obtained are in qualitative agreement with the well known statement that saddle cycles provide a detailed invariant characterization for dynamical systems of low intrinsic dimension (see e.g. [36]).

The fact that fluctuational escape from a non-hyperbolic attractor can be described in terms of transitions between just a few cycles opens up the pos-

sibility of an analytic estimate of the escape probability through an extension of the recent theory of the logarithmic susceptibility [19, 20] to the systems with limit cycles (M.I. Dykman and V.N. Smelyanskiy, private communication). In this approximation the escape probability from a non-hyperbolic attractor can be represented as the product of the probability of staying on the saddle cycle and the probability of a transition between cycles. The latter probability can be expressed analytically in terms of the known velocity of relaxation between limit cycles with rotational symmetry.

Simultaneously with measurement of the optimal path, we have found the optimal force by simple averaging of noisy realizations. The optimal force (Fig. 3(b)) consists of two parts corresponding to escape to the saddle cycles UC3 and UC1. It tends to zero after achievment of the saddle cycle UC1.

3 Fluctuational escape from a quasi-hyperbolic attractor

We now consider for comparison a fluctuational escape from the Lorenz attractor, which is a quasi-hyperbolic attractor consisting of unstable sets only. This system[37] is of interest because it describes e.g. convective fluid dynamics, as well as the single mode laser[38] and is often used as an example of a classical system with chaotic dynamics:

$$\begin{aligned} \dot{\mathbf{q}} &= \mathbf{K}(\mathbf{q}) + \mathbf{f}(t), \\ \mathbf{K} &= \{K_1, K_2, K_3\} = \{\sigma(q_2 - q_1), rq_1 - q_2 - q_1 q_3, q_1 q_2 - bq_3\}, \\ \mathbf{f}(t) &= \{0, 0, \xi(t)\}, \quad \langle \xi(t) \rangle = 0, \quad \langle \xi(t)\xi(0) \rangle = D\delta(t), \end{aligned} \tag{7}$$

For simplicity we consider the noise to act through the third equation only. For $\sigma = 10$, $b = 8/3$, $r = 24.08$, (7) has three attractors[37]: the stable points P_1 and P_2 and the Lorenz attractor (Fig. 4(a)). The stable manifolds of the saddle cycles L_1 and L_2 surround the stable points and they constitute boundaries between the chaotic and regular regimes in this region of phase space. The Lorenz attractor is an aggregate of integral curves going from L_1 to L_2 and back, the saddle point O, and its unstable one-dimensional manifolds (separatrices) $\mathit{\Gamma}_1$ and $\mathit{\Gamma}_2$. Note that the probability of trajectories passing near the separatrices and the cycles L_1 and L_2 is practically zero for the noise-free system. Like escape from a non-hyperbolic attractor, there is no theoretical prediction about the process of fluctuational escape from the Lorenz attractor. But the process is readily studied via numerical simulation and the method of analysis described above in relation to escape from a non-hyperbolic attractor. For definiteness, we examine escape to the stable point P_1. The averaged escape trajectory and corresponding averaged fluctuational force obtained in this way are shown in Fig. 4b.

We have found that escape occurs via the following scenario. The escape trajectory starts from the stable manifold of saddle point O. Under the

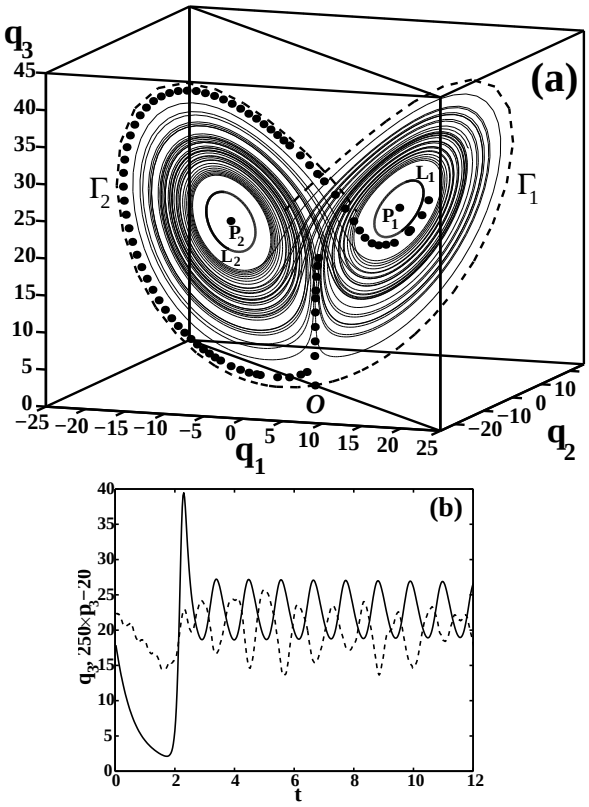

Fig. 4. (**a**) The structure of phase space of the Lorenz system. An escape trajectory measured by numerical simulation is indicated by the filled circles. (**b**) The averaged escape trajectory (full line) and the averaged fluctuational force (dashed line).

action of a fluctuation, an escape trajectory tends to point O along the two-dimensional stable manifold. Then, without reaching the saddle point O, the trajectory departs from it again, following a path close to the separatrix Γ_2, and falling into the neighborhood of the saddle cycle L_1. In the absence of the external force, the trajectory goes away from the cycle L_1, slowly untwisting. The fluctuational force induces a crossing through the saddle cycle, and the trajectory then relaxes to the stable point P_1. We can thus split the escape process into two parts: fluctuational and relaxational. Practically all of the fluctuational part belongs to the Lorenz attractor, and itself consists of two stages: first, the fluctuational force throws the trajectory as close as possible to the cycle L_1; secondly, the trajectory crosses this cycle under the action of fluctuations. The first stage is defined by the stable and unstable manifolds of the saddle point O, and the time-dependence of the fluctuational force is similar to that of the coordinate q_3 (Fig. 4b). During the second stage,

the fluctuations have a component which oscillates in anti-phase to the coordinate q_3. Because the trajectory of the noise-free system departs from the cycle L_1 very slowly, the fluctuational force inducing the crossing through the cycle may start to act at any time during a long interval. For this reason the averaged fluctuational force itself consists of a long oscillating function.

Practically all of the escape trajectory from the Lorenz attractor lies on the attractor itself. The role of the fluctuations is, first, the delivery of the trajectory to a seldom-visited area in the neighborhood of the saddle cycle L_1, and secondly, the inducing of a crossing cycle L_1. So we may conclude that the role of the fluctuations is different in this case, and the possibility of applying the Hamiltonian formalism will require a more detailed analysis of the crossing process.

In future investigations we plan to carry out more detailed statistical analyses of fluctuational trajectories and noise realizations to define the optimal force, because the simple averaging of noise realizations does not provide a very accurate result.

4 Summary

In summary, we have found that the mechanisms of escape from a non-hyperbolic attractor and a quasi-hyperbolic (Lorenz) attractor are quite different, and that the prehistory of escape reflects the different structure of their chaotic attractors. The escape process for the non-hyperbolic attractor is realized via several steps, which include transitions between low-period saddle-cycles co-existing in the system phase space. The escape from the Lorenz attractor consist of two qualitatively different stages: the first is defined by the stable and unstable manifolds of the saddle center point, and lies on the attractor; the second is the escape itself, crossing the saddle boundary cycle surrounding the stable point attractor. The corresponding optimal force was measured in both cases. We have shown that the mechanism of escape from the non-hyperbolic attractor may be amenable to a theoretical analysis within the framework of the Hamiltonian approach. Finally, note that our central results were obtained via an *experimental* definition of optimal paths, confirming our experimental approach as a powerful instrument for investigating noise-induced escape from complex attractors.

5 Acknowledgements

The work was supported by the Engineering and Physical Sciences Research Council (UK) under grant No. GR/L99562, by INTAS under grants Nos. YSF 99-3920 and 97-0574 and by the Royal Society of London.

References

1. Kifer Yu. (1989) Attractors via random perturbations. Commun. Math. Phys. **121**, 445-455; Arnold L. (1998) Random dynamical systems. Springer, Berlin; Schroer C.G., Ott E., Yorke J.A. (1998) Effect of noise on nonhyperbolic chaotic attractors. Phys. Rev. Lett. **81**, 1397—1400
2. Anishchenko V.S. (1995) Dynamical chaos: models and experiments. World Scientific, Singapore
3. Schimansky-Geier L., Herzel H. (1993) Positive Lyapunov exponents in the Kramers oscillator. J. Stat.Phys. **70**, 141-147.
4. Schive W.C. and Bulsara A.R. (1990) Multiplicative noise and homoclinic crossing: Chaos. Phys. Rev. A **41**, 1172–1174
5. Matsumoto K., Tsuda I. (1983) Noise induced order. J. Stat. Phys. **31**, 111—127
6. Fedchenia I.I., Mannella R., McClintock P.V.E., Stein N.D. and Stocks N.G. (1992) Influence of noise on periodic attractors in the Lorenz model: Zero-frequency spectral peaks and chaos. Phys. Rev. A **46**, 1769–1774
7. Bag B.C. and Ray D.S. (2000) Quantum noise induced chaotic oscillations. Phys. Rev. E **41**, 1172–1174
8. Grassberger P. (1989) Noise-induced escape from attractors. J. Phys. A **22**, 3283–3290
9. Graham R., Hamm A., Tel T. (1991) Nonequilibrium potentials for dynamical systems with fractal attractors or repellers. Phys. Rev. Lett. **66**, 3089–3092
10. Kautz R. L. (1996) Noise, chaos, and the Josephson standard. Rep. Prog. Phys. **59**, 935-992
11. Faure P., Korn H. (1997) A nonrandom dynamic component in the synaptic noise of a central neuron. Proc. Natl. Acad. Sci. USA. **94**, 6506–6511
12. Arimondo E., Hennequin D., Glorieux P. (1991) Noisy dynamics in optically bistable systems. in: McClintock P.V.E., Moss F. (Eds.) Noise in Nonlinear Dynamical Systems, Vol. 3, Cambridge university press, Cambridge, 119–158
13. Dykman M. I., McClintock P. V. E., Smelyanskiy V.N., Stein N.D., Stocks N.G. (1992) Optimal paths and the prehistory problem for large fluctuations in noise driven systems. Phys. Rev. Let. **68**, 2718–2721
14. Dykman M. I., Luchinsky D. G., McClintock P.V.E., Smelyanskiy V.N. (1996) Corrals and critical behavior of the distribution of fluctuational paths. Phys. Rev. Lett. **77**, 5229–5232
15. Luchinsky D. G., Maier R. G., Mannella R., McClintock P.V.E., Stein D.L. (1997) Experiments on critical phenomena in a noisy exit problem. Phys. Rev. Lett. **79**, 3117–3120
16. Luchinsky D. G. (1997) On the nature of large fluctuations in equilibrium systems: observation of an optimal force. J. Phys. A **30**, L577–L583
17. Onsager L., Machlup S. (1953) Fluctuations and irreversible processes. Phys. Rev. **91**, 1505–1512
18. Freidlin M. I., Wencel A. D. (1984) Random Perturbations in Dynamical Systems. Springer, New-York
19. Dykman M. I., Rabitz H., Smelyanskiy V. N., Vugmeister B. E. (1997) Resonant directed diffusion in nonadiabatically driven systems. Phys. Rev. Lett. **79**, 1178–1181

20. Smelyanskiy V. N., Dykman M. I., Rabitz H., Vugmeister B. E. (1997) Fluctuations, escape, and nucleation in driven systems: logarithmic susceptibility. Phys. Rev. Lett. **79**, 3113–3116
21. Luchinsky D. G., McClintock P. V. E. (1997) Irreversibility of classical fluctuations studied in analogue electrical circuits. Nature **389**, 463–466
22. Soskin S. M., Luchinsky D. G. et al. (1997) Zero-dispersion nonlinear resonance. Int. J. of Bifurc. and Chaos **7**, 923–936
23. Soskin S. M., Mannella R. et al. (1997) Chaos in periodically driven dissipative zero-dispersion systems in: Claeys C., Simoen E. (Eds.) Noise in Physical systems and 1/f fluctuations. Proc. of the 14th Int. Conf., IMEC. World Scientific, Leuven, Belgium, 351–354
24. Mannella R., Soskin S. M., McClintock P. V. E. (1998) Bifurcation analysis of zero-dispersion nonlinear resonance. Int. J. Bif. and Chaos **8**, 701–712
25. Afraimovich V. S., Shil'nikov L. P. (1983) Strange attractors and quasiattractors, in: Dynamics and Turbulence. Pitman, New York, 1–51
26. Kautz R. (1987) Activation energy for thermally induced escape from a basin of attraction. Phys. Lett. A. **125**, 315–319
27. Gibbs H. M., Hopf F. A., Kaplan D. L., Shoemaker R. L. (1981) Observation of chaos in optical bistability. J. Opt. Soc. America **71**, 367–375
28. Blackburn J. A., Smith H. J. T., Gronbech-Jensen N. (1996) Chaos and thermal noise in a Josephson junction coupled to a resonant tank. Phys. Rev. B. **53**, 14546–14551
29. Luchinsky D. G., McClintock P. V. E., Dykman M. I. (1998) Analogue studies of nonlinear systems. Rep. Prog. Phys. **61**, 889–997
30. Marsaglia G., Tsang W.-W. (1984) A fast, easily implemented method for sampling from decreasing or symmetric unimodal density-functions. SIAM J. Sci. Stat. Comput. **5**, 349–359
31. Ventcel' A. D., Freidlin M. I. (1970) On small random perturbations of dynamical systems. Uspehi. Mat. Nauk. **25**, 1–56
32. Dykman M. I., Krivoglaz M. A. (1979) Theory of the fluctuational transitions between the stable states of a nonlinear oscillator. Sov. Phys. - JETP. **50**, 30–37
33. Ludwig D. (1975) Persistence of dynamical systems under random perturbations. SIAM Rev. **17**, 605–640
34. Chinarov V. A., Dykman M. I., Smelyanskiy V. N. (1993) Dissipative corrections to escape probabilities of thermally nonequilibrium systems. Phys. Rev. E. **47**, 2448–2461
35. Feynman R. P., Hibbs A. R. (1965) Quantum mechanics and path integrals. McGraw-Hill
36. Grebogi C., Ott E., Yorke J. A. (1988) Unstable periodic orbits and the dimensions of multifractal chaotic attractors. Phys. Rev. A **37**, 1711–1724
37. Lorenz E.N. (1963) Deterministic nonperiodic flow. J. Atmos. Sci. **20**, 130–141
38. Graham R. (1989) Macroscopic potentials, bifurcations and noise in dissipative systems in: McClintock P.V.E., Moss F. (eds.) Noise in Nonlinear Dynamical Systems, Vol. 1, Cambridge university press, Cambridge, 225–278